

Giant Anomalous Hall and Nernst Effects in a Heavy Fermion Ferromagnet

Longfei Li,^{1,*} Shuyue Guan,^{1,*} Shengwei Chi,^{2,*} Jiawei

Li,¹ Xinxuan Lin,¹ Gang Xu,^{2,†} and Shuang Jia^{1,3,4,‡}

¹*International Center for Quantum Materials,*

School of Physics, Peking University, Beijing 100871, China

²*Wuhan National High Magnetic Field Center and School of Physics,
Huazhong University of Science and Technology, 430074, Wuhan, China*

³*Interdisciplinary Institute of Light-Element Quantum Materials
and Research Center for Light-Element Advanced Materials,*

Peking University, Beijing 100871, China

⁴*Hefei National Laboratory, Hefei 230088, China*

Abstract

The anomalous Hall and Nernst effects describe the voltage drop perpendicular to an applied current and temperature gradient due to the magnetization of a magnetic material. These effects can be utilized to measure the Berry curvature at the Fermi energy, and have potential applications in future electronic devices and thermoelectric energy conversion. In this paper, we report giant anomalous Hall conductivity and anomalous Nernst coefficient, as high as about $1000 \Omega^{-1} \text{ cm}^{-1}$ and $10 \mu\text{V K}^{-1}$, respectively, in a heavy fermion ferromagnet, CeCrGe_3 . This compound uniquely manifests strong hybridization between the $4f$ and conduction electrons, leading to a Kondo lattice state in the presence of ferromagnetic order. Unlike conventional topological semimetals in which the electron correlation is weak, CeCrGe_3 manifests a strong Berry curvature field of the heavy fermion with an extremely low Fermi energy. Our findings pave the way for exploring correlation-driven topological responses in a ferromagnetic Kondo lattice environment.

The investigation of the connection between electron correlation and topology is a pivotal goal in current condensed matter physics research [1, 2]. Strong correlations are necessary for the emergence of various topological phases, such as the fractional quantum Hall effect [3], topological Kondo insulators [4], and the anomalous fractional quantum Hall effect [5] that was recently discovered in experiments. Heavy fermions (HFs) are a well-known, strongly correlated electron system where the Kondo entanglement between the local moments of the f orbital electrons and the conduction electrons results in significant hybridization and the creation of spin singlets at low temperatures [6, 7]. The overlap of electronic states increases when f -electrons enter a conduction band, causing bandwidths to narrow drastically. In HF compounds, the characteristic energy of electronic states is orders of magnitude lower than that in ordinary metals, providing an ideal environment for investigating topological phases with strong correlations. Recent studies have indicated the presence of Weyl-Kondo semimetals and even topological semimetals without quasiparticles [8–11].

Magnetism can create complex topological phases and phenomena [12]. In particular, Weyl fermions and massive Dirac fermions have been observed in ferromagnetic (FM) materials when time-reversal symmetry is broken and there is spin-orbit coupling [13–15]. These topological magnets can exhibit massive quantum responses, such as the giant anomalous

* These authors contribute equally.

† Corresponding author: gangxu@hust.edu.cn

‡ Corresponding author: gwljiahuang@pku.edu.cn

Hall effect (AHE) and anomalous Nernst effect (ANE) [16, 17]. AHE and ANE are typically seen in magnetic materials as transverse electric and thermoelectric effects without an external magnetic field [18]. The Weyl and massive Dirac fermions can generate a giant Berry curvature, which produces much stronger anomalous effects compared to that in regular magnets [19]. Topological semimetals with giant ANE have shown potential for thermoelectric energy conversion [20–27]. However, the selection of materials for topological magnets is mainly limited to systems with weak interactions. It is yet to be explored whether an HF system can produce giant AHE and ANE from strongly correlated f electrons.

Cerium and ytterbium-based intermetallic compounds commonly exhibit paramagnetic and antiferromagnetic HF ground states [28–30]. However, the creation of FM HF materials is rare, with most reported magnets having either extremely low coherence temperatures or magnetic ordering temperatures [31–33], limiting the investigation of their topological responses. Recently, two FM uranium compounds were observed to have large AHE or ANE [34, 35]. Still, the relationship between electron correlation and topological effects remains unclear, and the radioactivity of uranium prevents the potential for any practical application. Our study identifies giant AHE and ANE in an HF ferromagnet, CeCrGe₃. The anomalous Hall conductivity (AHC) σ_{zx}^A was measured to be $983 \Omega^{-1} \text{ cm}^{-1}$, among the most significant observed in ferromagnets. Additionally, the anomalous Nernst coefficient reached $9.5 \mu\text{V K}^{-1}$ at 35 K. As comparison, the non- $4f$ -electron, isostructural, regular ferromagnet LaCrGe₃ shows a weak AHE. Our calculation reveals the presence of flat Ce- $4f$ electronic bands near the Fermi level, which hybridize with the Cr $3d$ electrons in CeCrGe₃, generating a strong Berry curvature field that aligns with the measured AHC. Furthermore, the anomalous Nernst conductivity (ANC) α_{zx}^A and anomalous thermal Hall coefficient follow the Mott relation and the anomalous Wiedemann-Franz (WF) law in the low-temperature limit, indicating that the giant effects can be attributed to the Berry curvature field of the heavy fermion with an extremely low Fermi energy (E_F).

CeCrGe₃ has a hexagonal perovskite, BaNiO₃-type structure that consists of chains of face-sharing Cr-centered Ge octahedra, aligned along the crystallographic c axis, and separated by the Ce atoms [36, 37] (as seen in Fig. 1 a). The Ge atoms on the nearby octahedra’s apex are strongly linked, forming a breathing kagome lattice in the ab plane. This lattice allows for strong bonding in all three dimensions of the structure. While the magnetic properties of polycrystalline CeCrGe₃ and LaCrGe₃ have been extensively studied [38–41], their

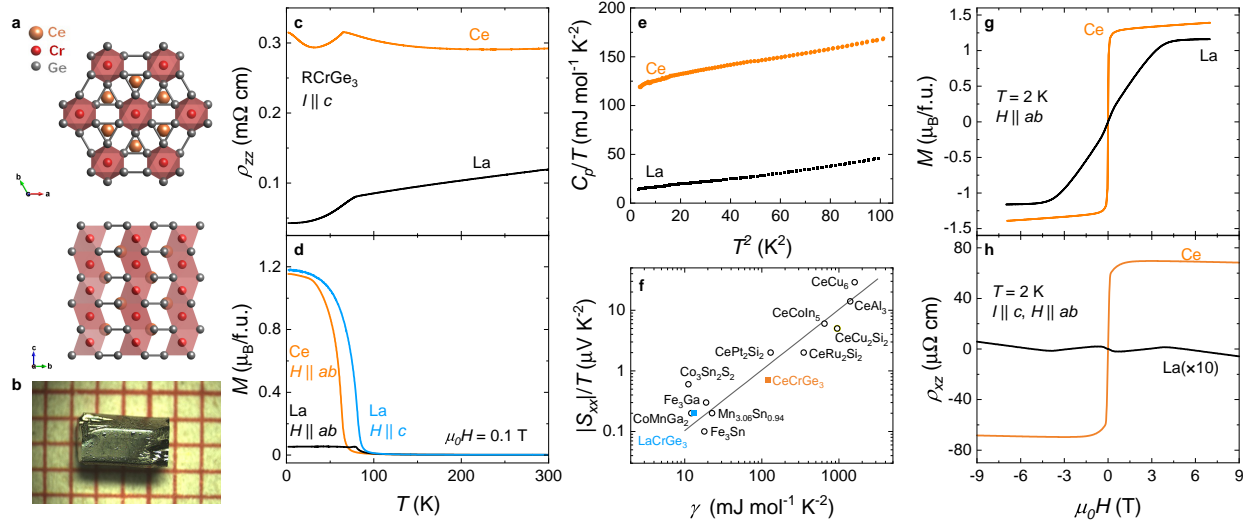


FIG. 1: Crystal structure and physical properties of CeCrGe_3 and LaCrGe_3 . **a**, Crystallographic structure of the hexagonal perovskite-type CeCrGe_3 . **b**, Photo of a single crystal of CeCrGe_3 . **c**, The temperature dependence of the longitudinal electric resistivity $\rho_{zz}(T)$ of CeCrGe_3 and LaCrGe_3 in zero field. **d**, The temperature dependence of the magnetization in an external magnetic field of 0.1 T applied in the crystallographic ab plane (black and orange curves) and c axis (the blue curve). **e**, Low-temperature specific heat of LaCrGe_3 and CeCrGe_3 , presented as C_p/T versus T^2 . **f**, Plot of $|S_{xx}|/T$ versus γ for representative Ce-based HF compounds and topological magnetic materials (Supplementary Information). **g**, **h**, The magnetic field dependence of the magnetization and the Hall resistivity at 2 K, with the field applied in the ab plane and the current applied along the c axis.

topological properties still require exploration. We utilized the self-flux method [42] to grow single crystals of CeCrGe_3 and LaCrGe_3 , resulting in crystals as large as $4 \times 2 \times 1 \text{ mm}^3$ (as seen in Fig. 1 b). Figures 1 c and d illustrate the temperature dependence of the electric resistivity $\rho_{zz}(T)$ in zero field and the magnetization in an external field of 0.1 T for the two compounds. Our findings are in line with previous reports on polycrystalline samples [36, 38, 40]. LaCrGe_3 with a $4f^0$ electronic configuration exhibits FM ordering below $T_C = 78 \text{ K}$ with an easy- c -axis anisotropy, while CeCrGe_3 with a $4f^1$ electronic configuration has $T_C = 65 \text{ K}$ with an easy- ab -plane anisotropy. The $\rho_{zz}(T)$ of LaCrGe_3 displays a typical metallic profile, whereas that of CeCrGe_3 shows Kondo-like behavior. Specifically, the resistivity increases with decreasing temperature down to T_C , followed by a drop down to 32

K. Below 32 K, the resistivity increases again. The high-temperature $-\ln T$ dependence is one of the Kondo lattice's characteristic features [43, 44], while the low-temperature upturn likely indicates some incoherent single-ion Kondo scattering, along with coherent Kondo scattering.

One of the distinctive features of HF systems is a significant Sommerfeld coefficient γ in the specific heat [28]. At low temperatures, the specific heat of both LaCrGe₃ and CeCrGe₃ is approximated by $C(T) = \gamma T + \beta T^3$ where γT is the electronic specific heat and βT^3 is the lattice (phonon) contribution (Fig. 1 e). The value of γ is 121 mJ mol⁻¹ K⁻² for CeCrGe₃, which is one order of magnitude larger than that for LaCrGe₃ (13 mJ mol⁻¹ K⁻²). The Kondo temperature can be roughly estimated as $T_K = \frac{R \ln 2}{\gamma_{\text{Ce}} - \gamma_{\text{La}}} = 50$ K for a doublet ground state, where R is the gas constant [45]. The carrier density of $n = -2.8 \times 10^{21}$ cm⁻³ and 3.4×10^{21} cm⁻³ was obtained from the magnitude of the ordinary Hall effect at 2 K (See SI, Fig. S1) for Ce and La, respectively. The Fermi temperatures (T_{F}) were estimated as 100 K and 1040 K for Ce and La, respectively, by using the equation [46] $T_{\text{F}} = \frac{\pi^2 k_{\text{B}} n}{2\gamma}$, where k_{B} is Boltzmann's constant. Assuming $\gamma = \frac{1}{3} \frac{k_{\text{B}}^2}{\hbar^2} k_{\text{F}} m^*$ and $E_{\text{F}} = k_{\text{B}} T_{\text{F}} = \frac{\hbar^2 k_{\text{F}}^2}{2m^*}$, we estimate the effective mass as $m^* = \left(\frac{9}{2} \gamma^2 \frac{\hbar^6}{k_{\text{B}}^5 T_{\text{F}}}\right)^{\frac{1}{3}} = 83 m_e$, which is consistent with the heavy nature of 4*f* electrons.

The Seebeck coefficients S_{zz} for the two compounds show a linear temperature dependence below 20 K (See SI, Fig. S2). The large slope of the $S_{zz}(T)$ of CeCrGe₃ at low temperatures correlates with the large γ , as observed in other correlated materials such as Ce-based HF compounds (Fig. 1 f) [47, 48]. All the above properties demonstrate that CeCrGe₃ is an HF ferromagnet, whereas LaCrGe₃ is a regular ferromagnet, albeit their similar magnetizations.

Figures 1 g and h illustrate the dependence of magnetization and Hall resistivity ρ_{xz} on the magnetic field for LaCrGe₃ and CeCrGe₃ at 2 K when the field was applied in the *ab* plane. LaCrGe₃, an easy-axis ferromagnet, displays a field-induced spin reorientation and a saturated magnetization of $M_{\text{sat}} = 1.1 \mu_{\text{B}}/\text{f.u.}$. On the other hand, CeCrGe₃, an easy-plane ferromagnet, has $M_{\text{sat}} = 1.3 \mu_{\text{B}}/\text{f.u.}$. The nearly identical magnetization in both compounds implies that the Ce 4*f* local moments have been fully Kondo screened at low temperatures, which is consistent with its HF state.

The Hall resistivity of CeCrGe₃ is two orders of magnitude higher than that of LaCrGe₃ at 2 K. In FM conductors, the Hall resistivity can be divided into normal and anomalous

contributions, as $\rho_H = R_H B + 4\pi R_s M$, where R_H and R_s are ordinary and anomalous Hall coefficients, respectively, B is the magnetic field, and M is the magnetization. The profiles of M and ρ_{xz} are nearly identical in CeCrGe_3 , leading to dominant anomalous contribution to the Hall resistivity. In contrast, the small signal of ρ_{xz} in LaCrGe_3 shows a complicated dependence on the field, which may indicate the presence of an additional spin orientation transition in the low field.

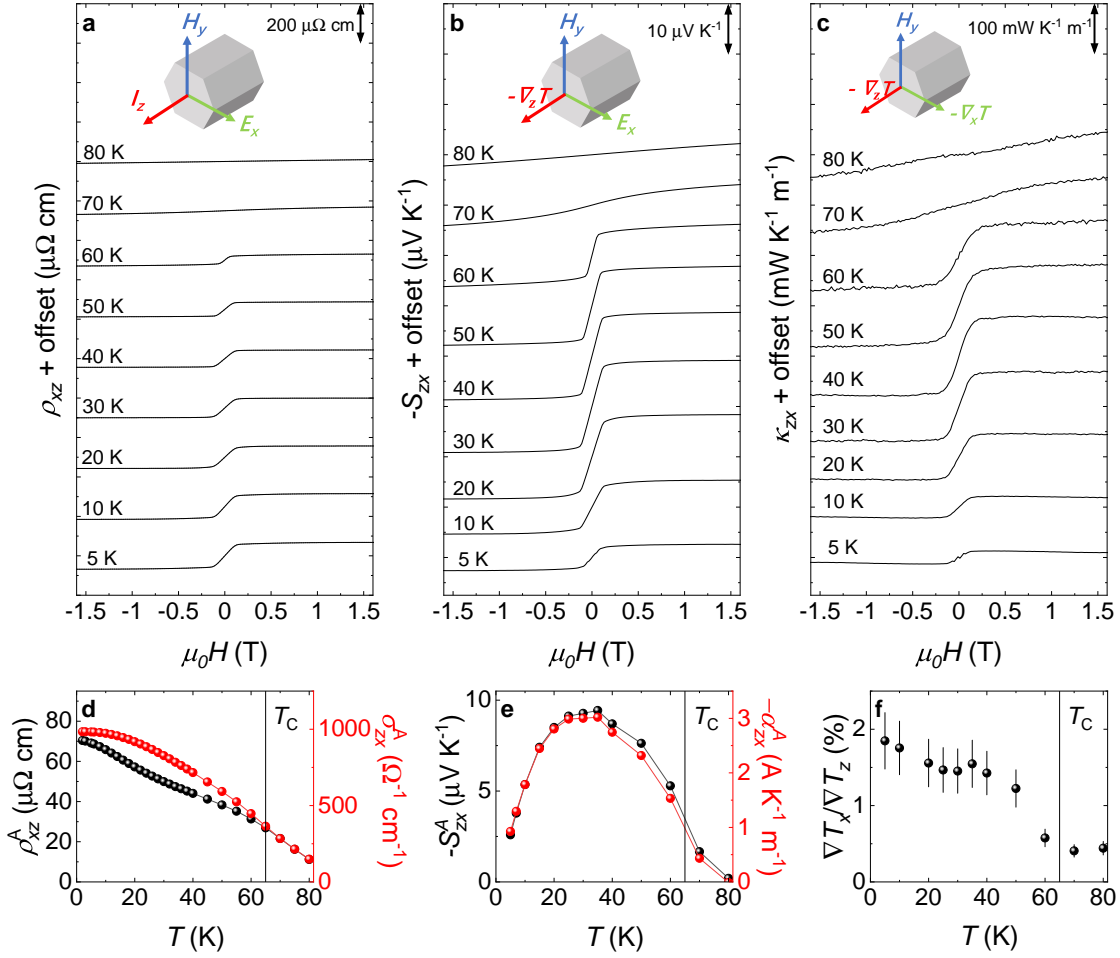


FIG. 2: Anomalous transport in CeCrGe_3 . **a-c**, The field dependence of the Hall resistivity $\rho_{xz}(H)$, the Nernst thermopower $-S_{zx}(H)$, and the thermal Hall conductivity $\kappa_{zx}(H)$ at representative temperatures. Curves are shifted vertically for clarity. **d**, The temperature dependence of the anomalous Hall resistivity ρ_{xz}^A (black, left axis) and the AHC σ_{zx}^A (red, right axis). **e**, The temperature dependence of the anomalous Nernst coefficient $-S_{zx}^A$ (black, left axis) and the ANC $-\alpha_{zx}^A$ (red, right axis), respectively. **f**, The temperature dependence of the anomalous thermal Hall angle $\nabla T_x / \nabla T_z$ (%).

We will now discuss the three transverse transport effects of charge and heat for CeCrGe₃. Figures 2 a-c demonstrate the Hall resistivity, Nernst thermopower, and thermal Hall conductivity, which are consistently with the $M(H)$ curves at various temperatures shown in Supplementary Information Fig. S3. At temperatures below 60 K, all three off-diagonal signals exhibit a sharp stage, corresponding to the FM $M(H)$. The anomalous off-diagonal signals disappear in the paramagnetic state when the temperature is above 80 K. We summarize the temperature dependence of the anomalous effects in Fig. 2 d-f. The anomalous Hall resistivity reaches its peak value of 70 $\mu\Omega$ cm at 2 K. Correspondingly, the AHC, $\sigma_{zx}^A = \frac{\rho_{xz}^A}{\rho_{xx}\rho_{zz} + (\rho_{xz}^A)^2}$, gradually increases with decreasing temperature and reaches its maximum value of 983 Ω^{-1} cm⁻¹ below 10 K, which is one of the largest values for FM metals. We notice that the change of σ_{zx}^A is irrelevant to the resistivity change below 30 K. Instead, the profile of σ_{zx}^A is similar to that for $M(T)$ in Fig. 1 c. In comparison, the AHC for LaCrGe₃ is only ~ 130 Ω^{-1} cm⁻¹ at 2 K, which is one order of magnitude smaller.

We have observed an unusually large anomalous Nernst coefficient $-S_{zx}^A$, which is as large as 9.5 $\mu\text{V K}^{-1}$ at a temperature of 35 K. This value is higher than most records [16, 20, 21, 49], and only UCo_{0.8}Ru_{0.2}Al has been reported to have a larger value [35]. At temperatures below 20 K, S_{zx}^A is directly proportional to temperature, down to the lowest temperature of 5 K that we could measure. As a result, the anomalous Nernst angle $\tan \theta_N = \left| \frac{S_{zx}^A}{S_{zz}^A} \right|$ is about 76% at 5 K. We calculated the ANC as $\alpha_{zx}^A = \sigma_{zx}^A S_{xx} + \sigma_{zz} S_{zx}^A$. As shown in Fig. 2 e, α_{zx}^A exactly follows the temperature dependence of S_{zx}^A because the second term $\sigma_{zz} S_{zx}^A$ overshadows the expression. $-\alpha_{zx}^A$ reaches its maximum value of 3.0 A K⁻¹ m⁻¹ at a temperature of 35 K, which is comparable to the highest values reported in other ferromagnets [26, 34, 49–51].

On the other hand, the anomalous thermal Hall conductivity reaches its maximum value of 81 mW K⁻¹ m⁻¹ at 40 K. This value is comparable to those recorded in topological magnets such as Mn₃Sn (40 mW K⁻¹ m⁻¹) [52] and Fe₃Sn₂ (86 mW K⁻¹ m⁻¹) [53] at room temperature. This giant anomalous thermal Hall effect leads to a significant anomalous thermal Hall angle of $\nabla T_x / \nabla T_z = \kappa_{zx} / \kappa_{xx}$, which reaches 2% at a temperature of 5 K.

We have compared the AHE and ANE of CeCrGe₃ with those of other ferromagnets, including various topological magnets, as shown in Fig. 3 a and b [16, 20, 21, 35, 49]. We have measured the anomalous Hall angle (AHA), $\tan \theta_{\text{AH}} = \left| \frac{\sigma_{\text{AH}}}{\sigma} \right|$, which measures the relative contribution of the anomalous Hall current with respect to the longitudinal current, is 22.5% at 2 K, among the largest values in various ferromagnets. For most magnetic

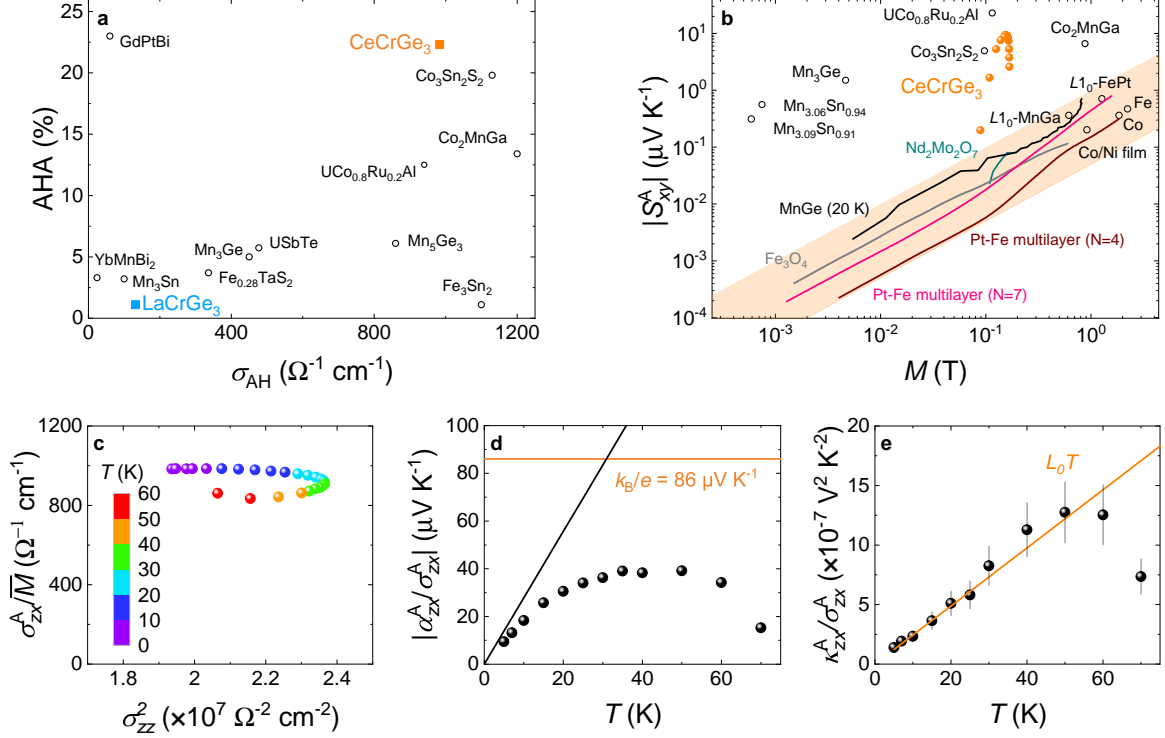


FIG. 3: Scaling of the anomalous transport coefficients. **a**, AHA as a function of σ_{AH} in topological magnetic materials. **b**, Anomalous Nernst coefficient $|S_{xy}^{\text{A}}|$ as a function of magnetization in magnetic materials. The $|S_{xy}^{\text{A}}|$ values for topological magnetic materials significantly surpass those for conventional magnetic materials (orange shaded region), in which $|S_{xy}^{\text{A}}|$ shows a linear dependence on the magnetization. **c**, $\sigma_{zx}^{\text{A}}/\bar{M}$ as a function of σ_{zz}^2 for CeCrGe₃, where the magnetization is normalized as $\bar{M} = M(T)/M_{\text{sat}}(T = 2 \text{ K})$. **d**, $|\alpha_{zx}^{\text{A}}/\sigma_{zx}^{\text{A}}|$ as a function of T for CeCrGe₃. The orange line indicates $k_{\text{B}}/e = 86 \mu\text{V K}^{-1}$, and the slope of the black line is $\frac{2\gamma}{3en}$. **e**, $\kappa_{zx}^{\text{A}}/\sigma_{zx}^{\text{A}}$ as a function of T for CeCrGe₃. The orange line represents the line with a slope of L_0 . The error bar is estimated as $\pm 20\%$ considering the uncertainty in the transport measurements and the samples' geometric factor.

materials, both σ_{AH} and σ are either large or small, so $\tan \theta_{\text{AH}}$ for these materials cannot be large. However, some materials, such as GdPtBi [54] and Co₃Sn₂S₂ [55], show exceptionally large $\tan \theta_{\text{AH}}$ with low carrier density ($n \sim 10^{19} \text{ cm}^{-3}$). CeCrGe₃ presents as another type of exception, as an HF ferromagnet with relatively high carrier density ($n \sim 10^{21} \text{ cm}^{-3}$). Figure 3 b shows the logarithmic plot of the anomalous Nernst coefficient versus magnetization for various magnets. The ANE is enhanced for topological metals such as Co₃Sn₂S₂ [55] and Co₂MnGa [56] than the empirical scaling relation with M as shown in the shaded region.

Nevertheless, only CeCrGe₃ and UCo_{0.8}Ru_{0.2}Al have the ANE in the order of 10 $\mu\text{V K}^{-1}$.

To investigate the AHE mechanism in CeCrGe₃, we conducted a scaling analysis of the AHC and longitudinal conductivity at different temperatures. Generally, the AHE is caused by an extrinsic skew scattering contribution resulting in a quadratic relationship between AHC and longitudinal conductivity ($\sigma_{zx}^A \sim \sigma_{zz}^2$) [57], or an intrinsic Berry-curvature-field contribution causing AHC to be independent of longitudinal conductivity [18, 19, 58, 59]. By considering the magnetization change from 2 K to the T_C , we scaled the AHC divided by the normalized magnetization $\overline{M} = M(T)/M_{\text{sat}}(T = 2 \text{ K})$ with σ_{zz}^2 , as shown in Fig. 3 c. Interestingly, the values of $\sigma_{zx}^A/\overline{M}$ are consistently around 1000 $\Omega^{-1} \text{ cm}^{-1}$, regardless of the change in σ_{zz} , indicating an intrinsic contribution. This intrinsic scaling relation of the AHE in CeCrGe₃ is unique in HF compounds, in which the skew scattering typically plays a vital role in a wide range [60–64].

We then examine the relationship between σ_{zx}^A and α_{zx}^A . Figure 3 d demonstrates that the ratio of $\alpha_{zx}^A/\sigma_{zx}^A$ is linearly dependent on the temperature at low temperatures, indicating the validity of the Mott relation, which will be elucidated in the following. However, at 40 K, the ratio reaches its maximum value of approximately $\frac{k_B}{2e}$ and then decreases with increasing temperature. It has been observed that the ratio usually increases monotonically with rising temperature and approaches the value of $\frac{k_B}{e}$ in a broad range of topological magnets [55, 56].

To verify the validity of the anomalous WF law, $\kappa_{zx}^A/\sigma_{zx}^A = L_0T$, we plotted the ratio $\kappa_{zx}^A/\sigma_{zx}^A$ versus T , as shown in Fig. 3 e. We found that the anomalous WF law is valid from 5 K up to 50 K, while the ratio is slightly deviated from the law at higher temperatures. It should be noted that the longitudinal thermal conductivity, κ_{zz} , is much larger than the WF law limit, indicating a dominant contribution from phonons even down to 5 K (See SI, Fig. S4). The validity of the anomalous WF law implies that the intrinsic contribution governs the anomalous transverse entropy and charge flows [52, 56, 65, 66].

The analysis above indicates that three anomalous effects are a result of the Berry-curvature-field effect on the electrons in CeCrGe₃. To understand how the 4*f* electrons of Ce and 3*d* electrons of Cr contribute to the strong Berry curvature field, we compared the electronic structures for LaCrGe₃ and CeCrGe₃ using density functional theory (DFT) in the local density approximation (LDA) [67]. Figures 4 a and b show that the biggest difference is some bands contributed by 4*f* orbitals appearing around the E_F in CeCrGe₃,

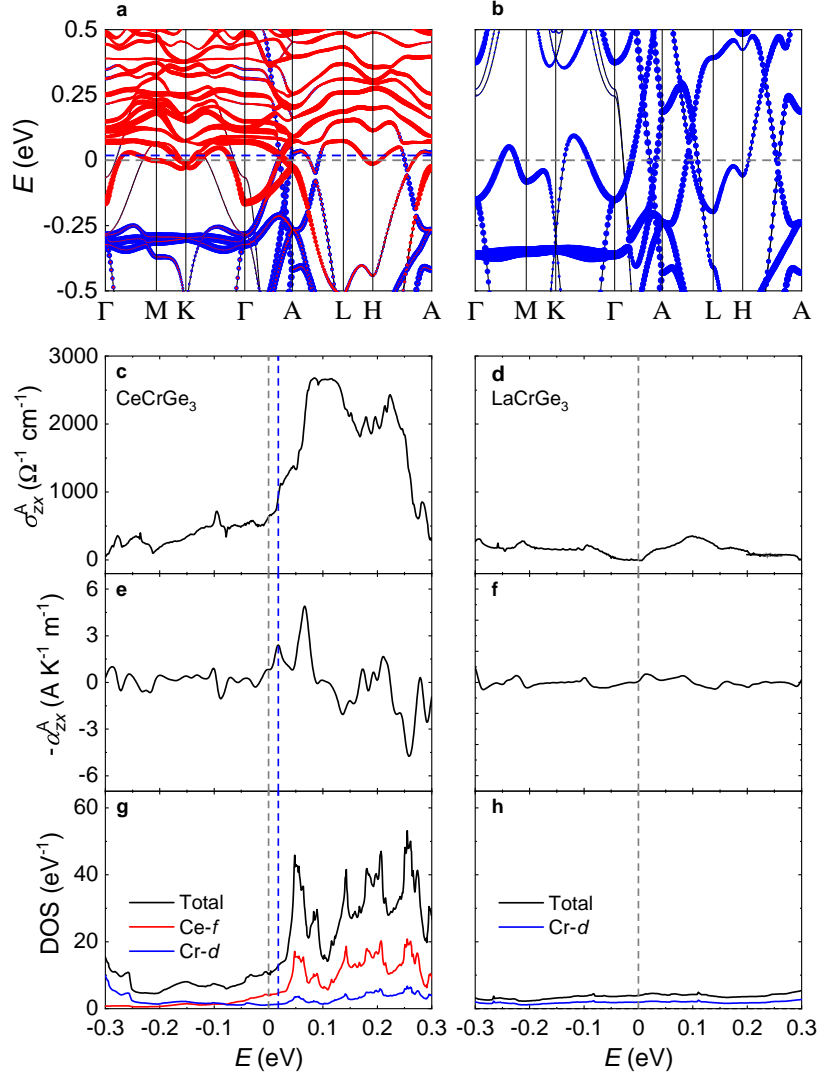


FIG. 4: DFT calculated electronic structures, AHC, and ANC for CeCrGe_3 and LaCrGe_3 . **a,b**, Band structures of CeCrGe_3 and LaCrGe_3 , respectively. The red and blue dots represent Ce- f and Cr- d orbital projections. **c-h**, Chemical potential dependency of AHC (σ_{zx}^A , $T = 0$ K), ANC ($-\alpha_{zx}^A$, $T = 35$ K), and total/partial DOS for CeCrGe_3 and LaCrGe_3 , respectively. Blue dashed lines in **a**, **c**, **e** and **g** correspond to the chemical potential at 18 meV.

leading to strong hybridization between the f and d electrons. As a result, CeCrGe_3 has a higher density of states (DOS) at E_F ($N_{E_F} = 10.7 \text{ eV}^{-1}$), dominated by the Ce- f and Cr- d orbitals, compared to LaCrGe_3 ($N_{E_F} = 3.9 \text{ eV}^{-1}$), where the Cr- d orbitals are prevalent. The electron mass enhancement parameter λ , estimated by comparing the bare Sommerfeld

coefficient γ_0 inferred from the DFT calculations to our measured values of γ , is 9.5 for CeCrGe₃, indicating a strong correlation of the electronic state.

Our calculation has shown that LaCrGe₃ and CeCrGe₃ have 4 and 19 pairs of Weyl points respectively, in an energy range of ± 20 meV near the E_F (refer to SI, Fig. S5). The intrinsic AHC has been determined by summing the Berry curvature of Bloch states over the occupied bands, and has been plotted as functions of the chemical potential in Fig. 4 c and d, respectively. At the E_F , the calculated AHC of CeCrGe₃ is $630 \Omega^{-1} \text{ cm}^{-1}$, and it increases to a higher value of $940 \Omega^{-1} \text{ cm}^{-1}$ at 18 meV, which is consistent with the experimental value. For LaCrGe₃, the calculated AHC is close to zero near the E_F for comparison.

It is worth noting that the calculated AHC for CeCrGe₃ reaches a value as high as $2700 \Omega^{-1} \text{ cm}^{-1}$ above 70 meV of the E_F , where the bands of the highest DOS consisting of the $4f$ orbitals of Ce dominate. This coincidence indicates that the $4f$ electrons of Ce play a crucial role in the strong Berry curvature field. Additionally, the calculation shows that the ANC value ($-\alpha_{zx}^A$) for CeCrGe₃ reaches $2.4 \text{ A K}^{-1} \text{ m}^{-1}$ at 18 meV higher than E_F , which is slightly less than the experimental value at 35 K ($3.0 \text{ A K}^{-1} \text{ m}^{-1}$). On the other hand, the calculated ANC for LaCrGe₃ is close to zero in an extensive energy range.

The skew scattering mechanism has been widely used to explain the anomalous Hall effect observed in HF systems [60–64]. In these systems, the Ce atom is considered as a local moment with a $4f^1$ configuration that periodically embeds in the conduction electron sea, leading to the formation of a Kondo lattice. In paramagnetic HF compounds, the Kondo resonance is disturbed by an external magnetic field due to Zeeman splitting, which causes skew scattering of the band electrons [63, 64]. However, this model is not strictly valid for the low-temperature regime ($T \ll T_K$), where a coherent HF band condenses out of the local moment landscape [63]. It should be noted that the validity of the model for the HF ferromagnets has not been verified as well.

The giant AHE and ANE of CeCrGe₃ demonstrate a distinct mechanism: a Berry-curvature-field mechanism that stems from the coherent HF bands. These highly correlated, renormalized bands manifest a narrow bandwidth and an extremely low E_F , characterized by the low T_K and T_F . Our comparative study of the AHE in CeCrGe₃ and LaCrGe₃ highlights the crucial role of the high-DOS, flat bands on the strong Berry curvature field. However, the large AHE does not guarantee a large ANE because the AHE is determined by the summation of the Berry curvature for all the occupied states, while the ANE is given by the

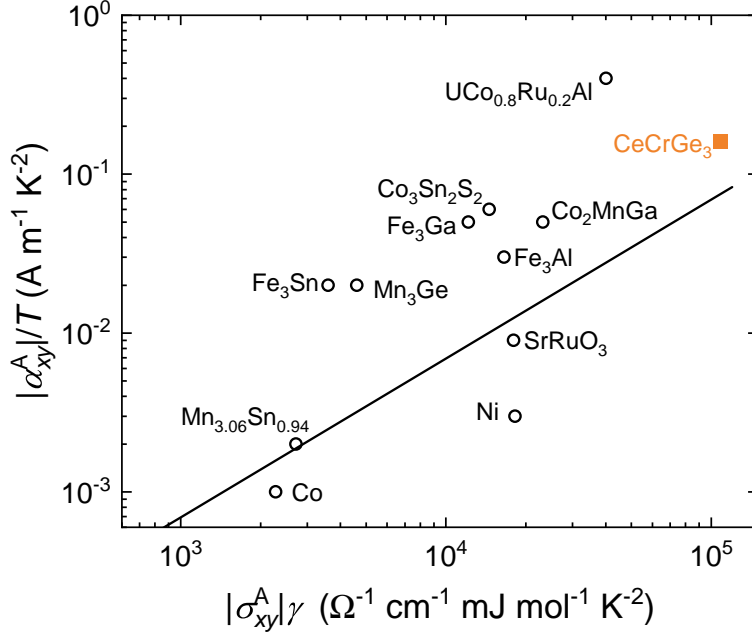


FIG. 5: The magnitude of the low-temperature $|\alpha_{xy}^A|/T$ as a function of $|\sigma_{xy}^A|\gamma$ for various magnets (Supplementary Information).

Berry curvature at the E_F [68]. For ordinary Nernst effect (ONE), Behnia *et al.* [48, 69] suggested that the ordinary Nernst coefficient can be expressed as $\nu = \frac{\pi^2 k_B k_B T}{3 e E_F} \mu$, where μ is the mobility. This expression indicates that ν/T can be significantly enhanced in the HF semimetals with a low T_F , which have the potential to be used for constructing a cryogenic Ettingshausen refrigerator [70]. However, for the ANE, a generic scaling law for various magnets is still absent.

In order to better understand the relationship between the AHE and ANE, we consider the Mott relation in various materials. Specifically, we look at $\frac{\alpha_{xy}^A}{T} \Big|_{T \rightarrow 0} = \frac{\pi^2 k_B^2}{3 e} \frac{\partial \sigma_{xy}^A}{\partial E} \Big|_{E=E_F}$, where we assume the most straightforward single-band approach and spherical Fermi surface. We replace the differential $\frac{\partial \sigma_{xy}^A}{\partial E} \Big|_{E=E_F}$ with the ratio $\frac{\sigma_{xy}^A}{E_F}$, leading to $\frac{\alpha_{xy}^A}{T} \Big|_{T \rightarrow 0} = \frac{\pi^2 k_B^2}{3 e E_F} \sigma_{xy}^A = \frac{2}{3en} \sigma_{xy}^A \gamma$. Also, this expression could be transformed to $\frac{\alpha_{xy}^A}{\sigma_{xy}^A} = \frac{2\gamma T}{3en} \Big|_{T \rightarrow 0}$, which is the black line in Fig. 3 d, depicting the Mott relation.

Figure 5 summarizes the magnitude of the low-temperature $|\alpha_{xy}^A|/T$ as a function of $|\sigma_{xy}^A|\gamma$ for various magnets (Supplementary Information), while the solid line represents the ratio of $\frac{2}{3}eN_A$ where N_A is the Avogadro constant. The data points are clustered around the line

regarding the rough single-band approximation and the uncertain values of n . This scaling relation of the ANE for a wide range of ferromagnets is reminiscent of that of the ONE and the thermal power for the HF compounds [47, 48, 71]. It indicates that the HF ferromagnets have the potential to demonstrate a giant intrinsic ANE at low temperatures.

The analysis above is only strictly valid at low temperatures. When the temperature is close to T_K , the Kondo resonance level is gradually decoherent; therefore, the heavy quasiparticles fade out. Zhu *et al.* [55] suggested that α_{xy}^A and S_{xy}^A are set by the summation of the Berry curvature over the thermal-wavelength cross-section of the Fermi surface, where the thermal-wavelength is defined as $\lambda_{dB} = \sqrt{\frac{2\pi\hbar^2}{m^*k_B T}}$. While the Fermi wavelength is $\lambda_F = \sqrt{\frac{2\pi^2\hbar^2}{m^*k_B T_F}}$, the ratio of the two wavelengths reaches a unity at 40 K for CeCrGe₃. About this temperature the band description of the heavy quasiparticles is no longer valid, leading to the invalid Mott relation, consistent with our observations.

Recent study discovers that the strong hybridization of f and conduction electrons in an FM Kondo lattice CeCo₂As₂ generates topological nodal loops near the Fermi level, which is a potent source of the Berry curvature field[72]. The giant intrinsic AHE in CeCrGe₃ suggests the existence of strongly correlated topological electronic structure which needs to be revealed by spectrum experiments in the future. Our work provides a novel paradigm for the strongly correlated, topological magnet, which demonstrates the heavy quasiparticle ($\sim 83 m_e$), giant intrinsic AHE ($\sim 1000 \Omega^{-1} \text{ cm}^{-1}$), and ANE ($\sim 10 \mu\text{V K}^{-1}$) at the same time. As the f -valence is extremely sensitive to external perturbations due to vanishing bandwidth, further transport experiments on CeCrGe₃ with hydrostatic pressure and chemical substitution would be particularly interesting. As suggested by previous studies, a quantum phase transition can be driven by moderate pressure [73]. Our findings provide a general guideline for searching for topological quantum phenomena in the HF magnets and also point out a new route for exploring thermoelectric energy conversion materials working in a cryogenic environment.

METHODS

Single crystal growth and magnetic measurements

High-quality single crystals of LaCrGe_3 and CeCrGe_3 were grown by the self-flux method. The raw materials of rare earth ingots, Cr ingots, and Ge ingots were mixed in a molar ratio of 15 : 15 : 85 and placed in a dry tantalum crucible, which was then sealed in a quartz ampoule under vacuum. The ampoule was placed in a furnace, slowly heated up to 1100°C over 7 hours, and held for 10 hours. It was then cooled down to the centrifugation temperature (around 850°C) where the excess self-flux was centrifuged. The crystal structure was examined by powder X-ray diffraction (PXR) using a Rigaku Mini-flux 600 diffractometer with $\text{Cu } K_\alpha$ radiation.

Magnetic properties were measured using the Quantum Design Magnetic Property Measurement System (MPMS-3), with the magnetic field applied along the crystallographic c axis and the ab plane, respectively.

Transport measurements

Transport properties were measured with the Quantum Design Physical Property Measurement System (PPMS-9) and the Oxford TeslatronPT-14T system. Longitudinal and Hall resistivity were measured using the standard four-probe method, and the Lake Shore Model 372 AC resistance bridge was used to collect the signals. Note that we use the convention $E_i = \rho_{ij}J_j$, which means ρ_{xz} is positive for hole carriers when the current is along the z axis and the field is along the y axis. Thermoelectric measurement was taken with a one-heater-three-thermometer setup using Cernox thermometers to monitor both the longitudinal and transverse temperature gradient simultaneously. The thermoelectric voltages were amplified with the EM DC Nanovolt Amplifier Model A10 and then collected by the Keithley Nanovoltmeter Model 2182A. Note that we use the convention $E_i = S_{ij}\partial_j T$.

DFT calculations

The first-principles calculations based on the DFT are implemented in the Vienna *ab initio* simulation package [74, 75] with the projector augmented wave method [76].

The cutoff energy for wave function expansion is set as 400 eV with $11 \times 11 \times 11$ k meshes. The LDA type of exchange-correlation potential [67] is utilized in our calculations. Maximally localized Wannier functions obtained from the WANNIER90 package [77], are used to derive the tight-binding model, which is subsequently employed for the calculation of the AHC and ANC. WannierTools [78] are used to calculate the AHC and find their Weyl points. The AHC and ANC were obtained by integrating the Berry curvature according to the formula [19, 79]:

$$\sigma_{\alpha\beta} = -\frac{e^2}{\hbar} \int_{\text{BZ}} \frac{d\mathbf{k}}{(2\pi)^3} \sum_n f(\varepsilon_{n\mathbf{k}}) \Omega_{n,\alpha\beta}(\mathbf{k}),$$

$$\alpha_{\alpha\beta} = \frac{ek_{\text{B}}}{\hbar} \int_{\text{BZ}} \frac{d\mathbf{k}}{(2\pi)^3} \sum_n s(\varepsilon_{n\mathbf{k}}) \Omega_{n,\alpha\beta}(\mathbf{k}).$$

The Berry curvature of band n with momentum \mathbf{k} is

$$\Omega_{n,\alpha\beta}(\mathbf{k}) = -2\hbar^2 \text{Im} \sum_{m(\neq n)} \frac{\langle n\mathbf{k} | v_\alpha | m\mathbf{k} \rangle \langle m\mathbf{k} | v_\beta | n\mathbf{k} \rangle}{(\varepsilon_{n\mathbf{k}} - \varepsilon_{m\mathbf{k}})^2},$$

where v_α is the velocity operator along the α direction, and $|n\mathbf{k}\rangle$ is the Bloch state with band index n and momentum \mathbf{k} . $f(\varepsilon) = (e^{(\varepsilon-\mu)/k_{\text{B}}T} + 1)^{-1}$ is the Fermi distribution function, and $s(\varepsilon)$ is given as $-f(\varepsilon) \ln f(\varepsilon) - (1 - f(\varepsilon)) \ln(1 - f(\varepsilon))$.

-
- [1] D. Pesin and L. Balents, Mott physics and band topology in materials with strong spin-orbit interaction, *Nature Physics* **6**, 376 (2010).
 - [2] Y. Tokura, Quantum materials at the crossroads of strong correlation and topology, *Nature Materials* **21**, 971 (2022).
 - [3] H. L. Stormer, D. C. Tsui, and A. C. Gossard, The fractional quantum hall effect, *Reviews of Modern Physics* **71**, S298 (1999).
 - [4] M. Dzero, K. Sun, V. Galitski, and P. Coleman, Topological kondo insulators, *Physical Review Letters* **104**, 106408 (2010).
 - [5] H. Park, J. Cai, E. Anderson, Y. Zhang, J. Zhu, X. Liu, C. Wang, W. Holtzmann, C. Hu, Z. Liu, T. Taniguchi, K. Watanabe, J.-H. Chu, T. Cao, L. Fu, W. Yao, C.-Z. Chang, D. Cobden, D. Xiao, and X. Xu, Observation of fractionally quantized anomalous hall effect, *Nature* **622**, 74 (2023).

- [6] A. C. Hewson, *The Kondo Problem to Heavy Fermions*, Cambridge Studies in Magnetism (Cambridge University Press, 1993).
- [7] P. Coleman, Heavy fermions: Electrons at the edge of magnetism, in *Handbook of Magnetism and Advanced Magnetic Materials* (John Wiley & Sons, Ltd, 2007) <https://onlinelibrary.wiley.com/doi/pdf/10.1002/9780470022184.hmm105>.
- [8] S. E. Grefe, H.-H. Lai, S. Paschen, and Q. Si, Weyl-kondo semimetals in nonsymmorphic systems, *Physical Review B* **101**, 075138 (2020).
- [9] H.-H. Lai, S. E. Grefe, S. Paschen, and Q. Si, Weyl-kondo semimetal in heavy-fermion systems, *Proceedings of the National Academy of Sciences* **115**, 93 (2018), <https://www.pnas.org/doi/pdf/10.1073/pnas.1715851115>.
- [10] S. Dzsaber, X. Yan, M. Taupin, G. Eguchi, A. Prokofiev, T. Shiroka, P. Blaha, O. Rubel, S. E. Grefe, H.-H. Lai, Q. Si, and S. Paschen, Giant spontaneous hall effect in a nonmagnetic weyl-kondo semimetal, *Proceedings of the National Academy of Sciences* **118**, e2013386118 (2021), <https://www.pnas.org/doi/pdf/10.1073/pnas.2013386118>.
- [11] H. Hu, L. Chen, C. Setty, M. Garcia-Diez, S. E. Grefe, A. Prokofiev, S. Kirchner, M. G. Vergniory, S. Paschen, J. Cano, and Q. Si, Topological semimetals without quasiparticles (2022), arXiv:2110.06182 [cond-mat.str-el].
- [12] Y. Tokura, K. Yasuda, and A. Tsukazaki, Magnetic topological insulators, *Nature Reviews Physics* **1**, 126 (2019).
- [13] E. Liu, Y. Sun, N. Kumar, L. Muechler, A. Sun, L. Jiao, S.-Y. Yang, D. Liu, A. Liang, Q. Xu, J. Kroder, V. Süß, H. Borrmann, C. Shekhar, Z. Wang, C. Xi, W. Wang, W. Schnelle, S. Wirth, Y. Chen, S. T. B. Goennenwein, and C. Felser, Giant anomalous hall effect in a ferromagnetic kagome-lattice semimetal, *Nature Physics* **14**, 1125 (2018).
- [14] L. Ye, M. Kang, J. Liu, F. von Cube, C. R. Wicker, T. Suzuki, C. Jozwiak, A. Bostwick, E. Rotenberg, D. C. Bell, L. Fu, R. Comin, and J. G. Checkelsky, Massive dirac fermions in a ferromagnetic kagome metal, *Nature* **555**, 638 (2018).
- [15] J.-X. Yin, W. Ma, T. A. Cochran, X. Xu, S. S. Zhang, H.-J. Tien, N. Shumiya, G. Cheng, K. Jiang, B. Lian, Z. Song, G. Chang, I. Belopolski, D. Multer, M. Litskevich, Z.-J. Cheng, X. P. Yang, B. Swidler, H. Zhou, H. Lin, T. Neupert, Z. Wang, N. Yao, T.-R. Chang, S. Jia, and M. Zahid Hasan, Quantum-limit chern topological magnetism in tbm₆sn₆, *Nature* **583**, 533 (2020).

- [16] T. Chen, T. Tomita, S. Minami, M. Fu, T. Koretsune, M. Kitatani, I. Muhammad, D. Nishio-Hamane, R. Ishii, F. Ishii, R. Arita, and S. Nakatsuji, Anomalous transport due to weyl fermions in the chiral antiferromagnets mn_3x , $\text{x}=\text{sn}$, ge , *Nature Communications* **12**, 572 (2021).
- [17] X. Xu, J.-X. Yin, W. Ma, H.-J. Tien, X.-B. Qiang, P. V. S. Reddy, H. Zhou, J. Shen, H.-Z. Lu, T.-R. Chang, Z. Qu, and S. Jia, Topological charge-entropy scaling in kagome chern magnet tbmn_6sn_6 , *Nature Communications* **13**, 1197 (2022).
- [18] N. Nagaosa, J. Sinova, S. Onoda, A. H. MacDonald, and N. P. Ong, Anomalous hall effect, *Reviews of Modern Physics* **82**, 1539 (2010).
- [19] D. Xiao, Y. Yao, Z. Fang, and Q. Niu, Berry-phase effect in anomalous thermoelectric transport, *Physical Review Letters* **97**, 026603 (2006).
- [20] M. Ikhlas, T. Tomita, T. Koretsune, M.-T. Suzuki, D. Nishio-Hamane, R. Arita, Y. Otani, and S. Nakatsuji, Large anomalous nernst effect at room temperature in a chiral antiferromagnet, *Nature Physics* **13**, 1085 (2017).
- [21] A. Sakai, Y. P. Mizuta, A. A. Nugroho, R. Sihombing, T. Koretsune, M.-T. Suzuki, N. Take-mori, R. Ishii, D. Nishio-Hamane, R. Arita, P. Goswami, and S. Nakatsuji, Giant anomalous nernst effect and quantum-critical scaling in a ferromagnetic semimetal, *Nature Physics* **14**, 1119 (2018).
- [22] S. N. Guin, P. Vir, Y. Zhang, N. Kumar, S. J. Watzman, C. Fu, E. Liu, K. Manna, W. Schnelle, J. Gooth, C. Shekhar, Y. Sun, and C. Felser, Zero-field nernst effect in a ferromagnetic kagome-lattice weyl-semimetal $\text{co}_3\text{sn}_2\text{s}_2$, *Advanced Materials* **31**, 1806622 (2019), <https://onlinelibrary.wiley.com/doi/pdf/10.1002/adma.201806622>.
- [23] A. Sakai, S. Minami, T. Koretsune, T. Chen, T. Higo, Y. Wang, T. Nomoto, M. Hirayama, S. Miwa, D. Nishio-Hamane, F. Ishii, R. Arita, and S. Nakatsuji, Iron-based binary ferromagnets for transverse thermoelectric conversion, *Nature* **581**, 53 (2020).
- [24] C. Fu, Y. Sun, and C. Felser, Topological thermoelectrics, *APL Materials* **8**, 040913 (2020), https://pubs.aip.org/aip/apm/article-pdf/doi/10.1063/5.0005481/14563406/040913.1_online.pdf.
- [25] Y. Pan, C. Le, B. He, S. J. Watzman, M. Yao, J. Gooth, J. P. Heremans, Y. Sun, and C. Felser, Giant anomalous nernst signal in the antiferromagnet ybmnbi_2 , *Nature Materials* **21**, 203 (2022).

- [26] T. Chen, S. Minami, A. Sakai, Y. Wang, Z. Feng, T. Nomoto, M. Hirayama, R. Ishii, T. Koretsune, R. Arita, and S. Nakatsuji, Large anomalous nernst effect and nodal plane in an iron-based kagome ferromagnet, *Science Advances* **8**, eabk1480 (2022), <https://www.science.org/doi/pdf/10.1126/sciadv.abk1480>.
- [27] S. Roychowdhury, M. Yao, K. Samanta, S. Bae, D. Chen, S. Ju, A. Raghavan, N. Kumar, P. Constantinou, S. N. Guin, N. C. Plumb, M. Romanelli, H. Borrmann, M. G. Vergniory, V. N. Strocov, V. Madhavan, C. Shekhar, and C. Felser, Anomalous hall conductivity and nernst effect of the ideal weyl semimetallic ferromagnet eucd2as2, *Advanced Science* **10**, 2207121 (2023), <https://onlinelibrary.wiley.com/doi/pdf/10.1002/advs.202207121>.
- [28] G. R. Stewart, Heavy-fermion systems, *Reviews of Modern Physics* **56**, 755 (1984).
- [29] G. R. Stewart, Non-fermi-liquid behavior in *d*- and *f*-electron metals, *Reviews of Modern Physics* **73**, 797 (2001).
- [30] G. R. Stewart, Addendum: Non-fermi-liquid behavior in *d*- and *f*-electron metals, *Reviews of Modern Physics* **78**, 743 (2006).
- [31] S. Süllo, M. C. Aronson, B. D. Rainford, and P. Haen, Doniach phase diagram, revisited: From ferromagnet to fermi liquid in pressurized CeRu₂Ge₂, *Physical Review Letters* **82**, 2963 (1999).
- [32] J. L. J., M. B. Fontes, A. D. Alvarenga, E. M. Baggio-Saitovitch, T. Burghardt, A. Eichler, and M. A. Continentino, Quantum critical behavior in a cept ferromagnetic kondo lattice, *Physical Review B* **72**, 035129 (2005).
- [33] M. Matusiak, A. Lipatov, A. Griбанov, and D. Kaczorowski, Anomalous nernst effect in the ferromagnetic kondo lattice ce3rhsi3, *Journal of Physics: Condensed Matter* **25**, 265601 (2013).
- [34] H. Siddiquee, C. Broyles, E. Kotta, S. Liu, S. Peng, T. Kong, B. Kang, Q. Zhu, Y. Lee, L. Ke, H. Weng, J. D. Denlinger, L. A. Wray, and S. Ran, Breakdown of the scaling relation of anomalous hall effect in kondo lattice ferromagnet usbte, *Nature Communications* **14**, 527 (2023).
- [35] T. Asaba, V. Ivanov, S. M. Thomas, S. Y. Savrasov, J. D. Thompson, E. D. Bauer, and F. Ronning, Colossal anomalous nernst effect in a correlated non-centrosymmetric kagome ferromagnet, *Science Advances* **7**, eabf1467 (2021), <https://www.science.org/doi/pdf/10.1126/sciadv.abf1467>.

- [36] H. Bie, O. Y. Zelinska, A. V. Tkachuk, and A. Mar, Structures and physical properties of rare-earth chromium germanides reCrGe_3 ($\text{re} = \text{La}, \text{Nd}, \text{Sm}$), *Chemistry of Materials* **19**, 4613 (2007), <https://doi.org/10.1021/cm071276+>.
- [37] B. Bosch-Santos, G. A. Cabrera-Pasca, E. L. Correa, B. S. Correa, T. N. S. Sales, K.-W. Moon, C. L. Dennis, Q. Huang, J. B. Leao, J. W. Lynn, and A. W. Carbonari, Magnetic and structural properties of the intermetallic $\text{Ce}_{(1-x)}\text{La}_x\text{CrGe}_3$ series of compounds, *Phys. Rev. Mater.* **5**, 114406 (2021).
- [38] D. Singh, M. M. Patidar, K. Suresh, and V. Ganesan, Metamagnetism in itinerant ferromagnetic CeCrGe_3 kondo system, *Physica B: Condensed Matter* **575**, 411701 (2019).
- [39] D. Das, A. Bhattacharyya, V. K. Anand, A. D. Hillier, J. W. Taylor, T. Gruner, C. Geibel, D. T. Adroja, and Z. Hossain, Muon spin relaxation study on itinerant ferromagnet CeCrGe_3 and the effect of Ti substitution on magnetism of CeCrGe_3 , *Journal of Physics: Condensed Matter* **27**, 016004 (2014).
- [40] D. Das, S. Nandi, I. da Silva, D. T. Adroja, and Z. Hossain, Neutron diffraction study on heavy-fermion compound CeCrGe_3 , *Physical Review B* **94**, 174415 (2016).
- [41] J. Cadogan, P. Lemoine, B. R. Slater, A. Mar, and M. Avdeev, Neutron diffraction study of the hexagonal perovskite-type compound LaCrGe_3 , in *Solid Compounds of Transition Elements II*, Solid State Phenomena, Vol. 194 (Trans Tech Publications Ltd, 2013) pp. 71–74.
- [42] X. Lin, V. Taufour, S. L. Bud'ko, and P. C. Canfield, Suppression of ferromagnetism in the $\text{LaV}_x\text{Cr}_{1-x}\text{Ge}_3$ system, *Physical Review B* **88**, 094405 (2013).
- [43] D. Das, T. Gruner, H. Pfau, U. B. Paramanik, U. Burkhardt, C. Geibel, and Z. Hossain, Heavy fermion and kondo lattice behavior in the itinerant ferromagnet CeCrGe_3 , *Journal of Physics: Condensed Matter* **26**, 106001 (2014).
- [44] S. Jang, J. D. Denlinger, J. W. Allen, V. S. Zapf, M. B. Maple, J. N. Kim, B. G. Jang, and J. H. Shim, Evolution of the kondo lattice electronic structure above the transport coherence temperature, *Proceedings of the National Academy of Sciences* **117**, 23467 (2020), <https://www.pnas.org/doi/pdf/10.1073/pnas.2001778117>.
- [45] Z. Fisk, J. Thompson, and H. Ott, Heavy-electrons: New materials, *Journal of Magnetism and Magnetic Materials* **76-77**, 637 (1988).
- [46] K. Behnia, *Fundamentals of Thermoelectricity* (Oxford University Press, 2015).
- [47] K. Behnia, The nernst effect and the boundaries of the fermi liquid picture, *Journal of Physics:*

- Condensed Matter **21**, 113101 (2009).
- [48] K. Behnia, D. Jaccard, and J. Flouquet, On the thermoelectricity of correlated electrons in the zero-temperature limit, *Journal of Physics: Condensed Matter* **16**, 5187 (2004).
- [49] H. Yang, W. You, J. Wang, J. Huang, C. Xi, X. Xu, C. Cao, M. Tian, Z.-A. Xu, J. Dai, and Y. Li, Giant anomalous nernst effect in the magnetic weyl semimetal $\text{Co}_3\text{Sn}_2\text{S}_2$, *Phys. Rev. Mater.* **4**, 024202 (2020).
- [50] Y. Li, J. Zhou, M. Li, L. Qiao, C. Jiang, Q. Chen, Y. Li, Q. Tao, and Z.-A. Xu, Enhanced anomalous nernst effect by tuning the chemical potential in the topological kagome ferromagnet Fe_3Sn_2 , *Phys. Rev. Appl.* **19**, 014026 (2023).
- [51] S. N. Guin, K. Manna, J. Noky, S. J. Watzman, C. Fu, N. Kumar, W. Schnelle, C. Shekhar, Y. Sun, J. Gooth, and C. Felser, Anomalous nernst effect beyond the magnetization scaling relation in the ferromagnetic heusler compound Co_2MnGa , *NPG Asia Materials* **11**, 16 (2019).
- [52] X. Li, L. Xu, L. Ding, J. Wang, M. Shen, X. Lu, Z. Zhu, and K. Behnia, Anomalous nernst and righi-leduc effects in Mn_3Sn : Berry curvature and entropy flow, *Physical Review Letters* **119**, 056601 (2017).
- [53] H. Zhang, C. Q. Xu, and X. Ke, Topological nernst effect, anomalous nernst effect, and anomalous thermal hall effect in the dirac semimetal Fe_3Sn_2 , *Physical Review B* **103**, L201101 (2021).
- [54] C. Shekhar, N. Kumar, V. Grinenko, S. Singh, R. Sarkar, H. Luetkens, S.-C. Wu, Y. Zhang, A. C. Komarek, E. Kampert, Y. Skourski, J. Wosnitza, W. Schnelle, A. McCollam, U. Zeitler, J. Kübler, B. Yan, H.-H. Klauss, S. S. P. Parkin, and C. Felser, Anomalous hall effect in weyl semimetal half-heusler compounds RPtBi ($r = \text{gd}$ and nd), *Proceedings of the National Academy of Sciences* **115**, 9140 (2018), <https://www.pnas.org/doi/pdf/10.1073/pnas.1810842115>.
- [55] L. Ding, J. Koo, L. Xu, X. Li, X. Lu, L. Zhao, Q. Wang, Q. Yin, H. Lei, B. Yan, Z. Zhu, and K. Behnia, Intrinsic anomalous nernst effect amplified by disorder in a half-metallic semimetal, *Physical Review X* **9**, 041061 (2019).
- [56] L. Xu, X. Li, L. Ding, T. Chen, A. Sakai, B. Fauqué, S. Nakatsuji, Z. Zhu, and K. Behnia, Anomalous transverse response of Co_2MnGa and universality of the room-temperature $\alpha_{ij}^A/\sigma_{ij}^A$ ratio across topological magnets, *Physical Review B* **101**, 180404 (2020).
- [57] Y. Tian, L. Ye, and X. Jin, Proper scaling of the anomalous hall effect, *Physical Review Letters* **103**, 087206 (2009).

- [58] S. Onoda, N. Sugimoto, and N. Nagaosa, Quantum transport theory of anomalous electric, thermoelectric, and thermal hall effects in ferromagnets, *Physical Review B* **77**, 165103 (2008).
- [59] S. Onoda, N. Sugimoto, and N. Nagaosa, Intrinsic versus extrinsic anomalous hall effect in ferromagnets, *Physical Review Letters* **97**, 126602 (2006).
- [60] P. Coleman, P. W. Anderson, and T. V. Ramakrishnan, Theory for the anomalous hall constant of mixed-valence systems, *Physical Review Letters* **55**, 414 (1985).
- [61] A. Fert and P. M. Levy, Theory of the hall effect in heavy-fermion compounds, *Physical Review B* **36**, 1907 (1987).
- [62] H. Kontani and K. Yamada, Theory of anomalous hall effect in heavy fermion system, *Journal of the Physical Society of Japan* **63**, 2627 (1994), <https://doi.org/10.1143/JPSJ.63.2627>.
- [63] S. Nair, S. Wirth, S. Friedemann, F. Steglich, Q. Si, and A. J. Schofield, Hall effect in heavy fermion metals, *Advances in Physics* **61**, 583 (2012).
- [64] Y.-f. Yang, Anomalous hall effect in heavy electron materials, *Physical Review B* **87**, 045102 (2013).
- [65] Y. Onose, Y. Shiomi, and Y. Tokura, Lorenz number determination of the dissipationless nature of the anomalous hall effect in itinerant ferromagnets, *Physical Review Letters* **100**, 016601 (2008).
- [66] Y. Shiomi, Y. Onose, and Y. Tokura, Effect of scattering on intrinsic anomalous hall effect investigated by lorenz ratio, *Physical Review B* **81**, 054414 (2010).
- [67] J. P. Perdew and A. Zunger, Self-interaction correction to density-functional approximations for many-electron systems, *Physical Review B* **23**, 5048 (1981).
- [68] D. Xiao, M.-C. Chang, and Q. Niu, Berry phase effects on electronic properties, *Reviews of Modern Physics* **82**, 1959 (2010).
- [69] K. Behnia, M.-A. Méasson, and Y. Kopelevich, Nernst effect in semimetals: The effective mass and the figure of merit, *Physical Review Letters* **98**, 076603 (2007).
- [70] J. Mao, G. Chen, and Z. Ren, Thermoelectric cooling materials, *Nature Materials* **20**, 454 (2021).
- [71] K. Behnia and H. Aubin, Nernst effect in metals and superconductors: a review of concepts and experiments, *Reports on Progress in Physics* **79**, 046502 (2016).
- [72] Z.-J. Cheng, Y. Huang, P. Zheng, L. Chen, T. A. Cochran, H. Hu, J.-X. Yin, X. P. Yang, M. S. Hossain, Q. Zhang, I. Belopolski, R. Liu, G. Cheng, M. Hashimoto, D. Lu, X. Xu, H. Zhou,

- W. Ma, G. Chang, N. Yao, Z. Yin, M. Z. Hasan, and S. Jia, Observation of kondo lattice and kondo-enhanced anomalous hall effect in an itinerant ferromagnet (2023), arXiv:2302.12113 [cond-mat.str-el].
- [73] V. Taufour, U. S. Kaluarachchi, R. Khasanov, M. C. Nguyen, Z. Guguchia, P. K. Biswas, P. Bonfà, R. De Renzi, X. Lin, S. K. Kim, E. D. Mun, H. Kim, Y. Furukawa, C.-Z. Wang, K.-M. Ho, S. L. Bud'ko, and P. C. Canfield, Ferromagnetic quantum critical point avoided by the appearance of another magnetic phase in LaCrGe_3 under pressure, *Physical Review Letters* **117**, 037207 (2016).
- [74] G. Kresse and J. Furthmüller, Efficiency of ab-initio total energy calculations for metals and semiconductors using a plane-wave basis set, *Computational Materials Science* **6**, 15 (1996).
- [75] G. Kresse and J. Furthmüller, Efficient iterative schemes for ab initio total-energy calculations using a plane-wave basis set, *Physical Review B* **54**, 11169 (1996).
- [76] P. E. Blöchl, Projector augmented-wave method, *Physical Review B* **50**, 17953 (1994).
- [77] A. A. Mostofi, J. R. Yates, G. Pizzi, Y.-S. Lee, I. Souza, D. Vanderbilt, and N. Marzari, An updated version of wannier90: A tool for obtaining maximally-localised wannier functions, *Computer Physics Communications* **185**, 2309 (2014).
- [78] Q. Wu, S. Zhang, H.-F. Song, M. Troyer, and A. A. Soluyanov, Wanniertools: An open-source software package for novel topological materials, *Computer Physics Communications* **224**, 405 (2018).
- [79] X. Wang, J. R. Yates, I. Souza, and D. Vanderbilt, Ab initio calculation of the anomalous hall conductivity by wannier interpolation, *Physical Review B* **74**, 195118 (2006).